JPE 16-4-28

http://dx.doi.org/10.6113/JPE.2016.16.4.1541
ISSN(Print): 1598-2092 / ISSN(Online): 2093-4718

Comparison and Study of Active and Hybrid Power Filters for Compensation of Grid Harmonics

Bryan Gutierrez* and Sang-Shin Kwak†

*,†School of Electrical and Electronics Engineering, Chung-Ang University, Seoul, Korea

Abstract

This paper presents a theoretical analysis and comparisons of active power filter (APF) and hybrid power filter (HPF) systems, given terminal constraints of harmonic compensations in nonlinear loads. Despite numerous publications for the two types of filters, the features and differences between them have not been clearly explained. This paper presents a detailed analysis of the operations of a HPF inverter along with those of passive power filters (PPFs). It also includes their effects on the power factor at the grid. In addition, a theoretical analysis and a systematic comparison between the APF and HPF systems are addressed based on system parameters such as the source voltage, output power, reactive component size, and power factor at the grid terminals. The converter kVA ratings and dc-link voltage requirements for both topologies are considered in the presented comparisons.

Key words: Active power filter, Diode rectifier, Harmonic compensation, Hybrid power filter, Power factor

I. INTRODUCTION

Diode rectifiers, which are the most common nonlinear loads, create harmonic problems in power distribution systems, leading to restricted norms such as the IEEE-519 standards for power quality. Initially, passive power filters (PPFs) composed of several three-phase LC circuits tuned at the most relevant harmonics were implemented to reduce harmonic components. However, PPFs have drawbacks such as resonances, tuning problems, fixed compensation capability and bulky size [1]. On the other hand, active power filters (APFs) have become an attractive solution to improve the power quality and enhance the performance of PPFs [2]-[8]. However, APFs suffer from the disadvantage of expensive large-scale implementation mostly due to the high dc-link voltage of the inverter [9], [10]. Recently, hybrid power filters (HPFs), made of an APF inverter in series with a single frequency tuned PPF, have been introduced to reduce the dc-link voltage of the inverter, which in turn lowers the cost of large-scale applications [11], [12]. Applications of HPF systems and diverse control strategies of HPFs have been investigated [13]-[19]. However, despite numerous studies on HPFs, a detailed analysis of the HPF inverter rating and its relationship to the PPF design is an important omission in the literature. In addition, a comprehensive comparative analysis between APF and the HPF systems has not been done.

The objective of this paper is to clearly address and compare the features and requirements of APF and HPF systems. A comprehensive and detail rating analysis is presented for APF and the HPF inverters with a typical diode rectifier load. This is done based on mathematical derivations. The effects of non-instantaneous commutations of the input current in the diode rectifier are considered, because non-instantaneous commutations with the input inductance are more feasible in practice. The HPF inverter and power factor of the grid terminals are analysed in terms of practical system parameters such as the source voltage, the output power, the reactive components of the PPF, and the ac inductance of the diode rectifier. Based on the analysis of APF and HPF systems, the kVA ratings and dc-link voltage levels of APF and HPF inverters are compared according to the system parameters.

II. APF AND HPF SYSTEMS AND NONLINEAR LOADS

Fig. 1 shows APF and HPF systems with a nonlinear load represented by a three-phase six-pulse diode rectifier with an ac inductance (L_{ac}) and a dc-side current (I_{dc}), respectively. In

Manuscript received Sep. 3, 2015; accepted Mar. 26, 2016
Recommended for publication by Associate Editor Po-Tai Cheng.
†Corresponding Author: sskwak@cau.ac.kr
Tel: +82-2-820-5346, Fax: +82-2-820-1584, Chung-Ang University
*School of Electrical and Electronics Engineering, Chung-Ang University, Korea

the APF system, the APF inverter supplies both the reactive power and the harmonic power, which leads to a unity power factor at the grid terminals. On the other hand, the HPF inverter compensates for harmonic power by only providing harmonic currents, while the PPF is responsible for the uncontrolled reactive power compensation. Therefore, the unity power factor operation at the grid with the HPF system is not guaranteed with varying load conditions once the PPF is tuned.

For an analytical and fair comparison, both systems are analysed under the same grid and load conditions considering no semiconductor losses in the inverters and no resistive losses in the reactive components. The source phase voltage is given by the line-to-line rms voltage (V_{LL}) and the angular frequency ω ($\omega = 2\pi \times 50$) by:

$$v_s(\omega t) = \sqrt{2/3}\, V_{LL} \cos(\omega t)\,. \tag{1}$$

In addition, the nonlinear load current is described because the behaviour of the APF and the HPF inverters is considerably influenced by load conditions. Fig. 2 shows the source voltage (v_s), the load current (i_L), and the source current (i_S) flowing in the APF and HPF systems. Fig. 2 (a) shows v_s with i_L and its fundamental component i_{Lf}, along with the load displacement power factor (DPF) angle (φ) and the commutation interval (Δ).

Fig. 2(b) shows i_S after compensation operating at unity power factor since the APF compensates the harmonic and reactive power. Fig. 2(c) shows i_S after the compensation with the HPF having a power factor angle of θ since the HPF compensates only the reactive power. The commutations of the load current, as shown in Fig. 2(a), are not instantaneous as in the ideal cases owing to the presence of L_{ac}. In a commutation interval, the load current is [20]:

$$i_L(\omega t) = I_{dc} + \frac{V_{LL}}{\sqrt{2}\omega L_{ac}}\left[\cos\left(\frac{\pi}{3} - \omega t\right) - 1\right],\ \ \frac{\pi}{3} \le \omega t \le \frac{\pi}{3} + \Delta\,. \tag{2}$$

From (2) and Fig. 2 (a), the commutation interval is calculated by:

$$\Delta = \cos^{-1}\left(1 - \frac{\sqrt{2}\omega L_{ac} I_{dc}}{V_{LL}}\right). \tag{3}$$

Then, the load current drawn can be found employing the Fourier series analysis:

$$\begin{aligned} i_L(\omega t) = \frac{2\sqrt{3}I_{dc}}{\pi} \{ & M_L \cos(\omega t - \varphi) + \left(a_5 \cos(5\omega t) + b_5 \sin(5\omega t)\right) - \\ & \left(a_7 \cos(7\omega t) + b_7 \sin(7\omega t)\right) + \left(a_{11} \cos(11\omega t) + b_{11} \sin(11\omega t)\right) - \ldots \}\ \cdot \end{aligned} \tag{4}$$

where:

$$M_L = \frac{\sqrt{(\Delta/2)^2 + (\sin(\Delta)/2)^2 - \Delta \sin(\Delta)\cos(\Delta)/2}}{1 - \cos(\Delta)}$$

$$a_k = \frac{1}{2k(k+1)}\left[\frac{\sin((k+1)\Delta/2)}{\sin(\Delta/2)}\right]^2 - \frac{1}{2k(k-1)}\left[\frac{\sin((k-1)\Delta/2)}{\sin(\Delta/2)}\right]^2$$

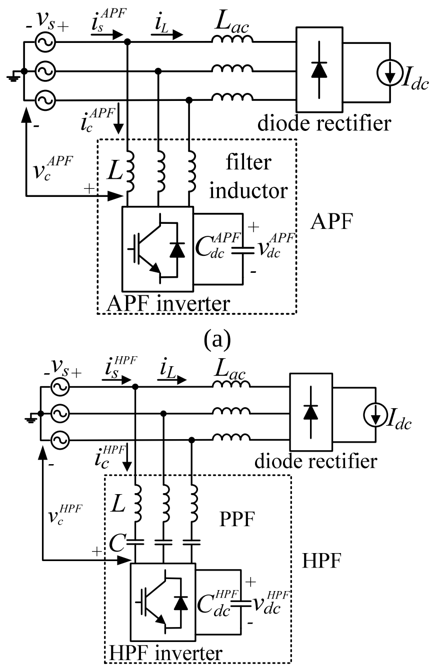

Fig. 1. Filtering systems of nonlinear loads with (a) APF and (b) HPF.

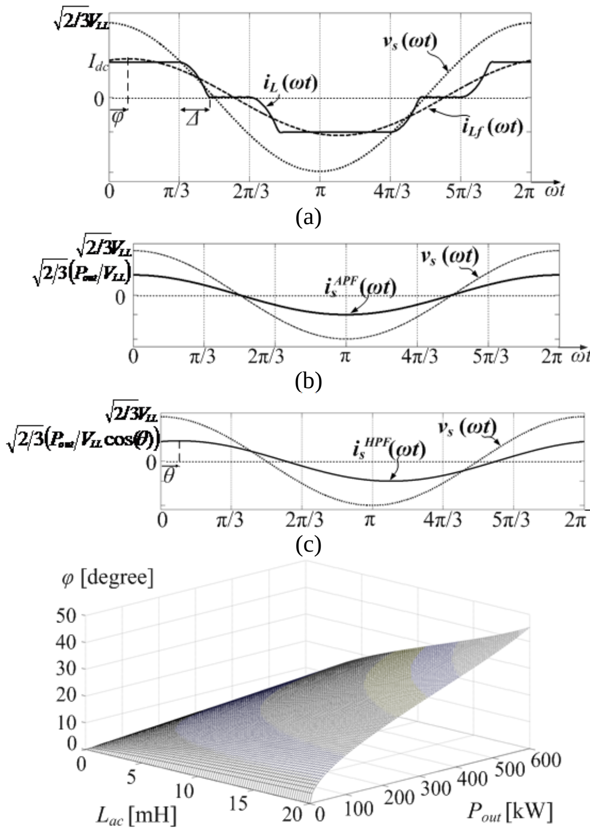

Fig. 2. (a) Source voltage and load current from diode rectifier with input inductance L_{ac}. (b) Source voltage and source current in APF system. (c) Source voltage and source current in HPF system. (d) Load DPF angle versus L_{ac} and P_{out} (V_{LL} = 3000 V).

$$b_k = \frac{\sin(\Delta(k-1))}{2k(k-1)(1-\cos(\Delta))} - \frac{\sin(\Delta(k+1))}{2k(k+1)(1-\cos(\Delta))},\; k = 5,7,11,13,...$$

Assuming that the switching devices and the reactive components in both APF and the HPF systems have no losses, I_{dc} can be related to P_{out} as:

$$I_{dc} = \frac{\pi P_{out}}{3\sqrt{2}V_{LL}M_L\cos(\varphi)}. \tag{5}$$

In addition, the load DPF angle, φ, shown in Fig. 2 (a) is derived from (4) as:

$$\varphi = \frac{\pi}{2} - \tan^{-1}\left(\frac{\sin^2(\Delta)}{\Delta - \sin(\Delta)\cos(\Delta)}\right). \tag{6}$$

From (3), (5), and (6), it is obvious that the angle φ depends on L_{ac} and P_{out}, which are directly associated with the load reactive power. Fig. 2 (d) is a plot of the load DPF angle versus L_{ac} and P_{out}. It can be seen that increasing L_{ac} and P_{out} increases the load reactive power, which in turn leads to a higher load DPF angle.

III. ANALYSIS OF THE KVA RATINGS OF APF AND HPF INVERTERS

In this section, analytical derivations for the kVA ratings of the inverters are presented by considering the characteristics of the nonlinear load and grid shown in the previous section.

A. kVA Rating Analysis of APF Inverter

Because the APF inverter delivers both reactive power and harmonic power to the diode rectifier, the source current is in phase with the source voltage. Therefore, the source current operating with the APF system shown in Fig. 2 (b) is given by:

$$i_s^{APF}(\omega t) = \sqrt{2/3}\left(P_{out}/V_{LL}\right)\cos(\omega t)\cdot \tag{7}$$

The kVA rating of the APF inverter can be expressed with the rms value of the current through the inverter and the rms value of the ac-side voltage of the inverter as:

$$S_{APF} = 3V_c^{APF}I_c^{APF}. \tag{8}$$

where I_c^{APF} and V_c^{APF} represent the rms value of the compensating current through the APF inverter and the rms value of the ac-side voltage of the inverter, respectively. From (4) and (7), the rms value of the compensating current generated by the inverter is derived as:

$$I_c^{APF} = \frac{P_{out}}{\sqrt{3}V_{LL}}\sqrt{\tan^2(\varphi) + \frac{K_1}{\left(M_L\cos(\varphi)\right)^2}} \tag{9}$$

where:

$$K_1 = \sum_{m=1}^{n/2}(a_k^2 + b_k^2)\;,\; k = 6m \mp 1.$$

The rms value of the ac-side voltage of the APF inverter can be calculated from Fig. 1 (a), (1), (4), and (7) as:

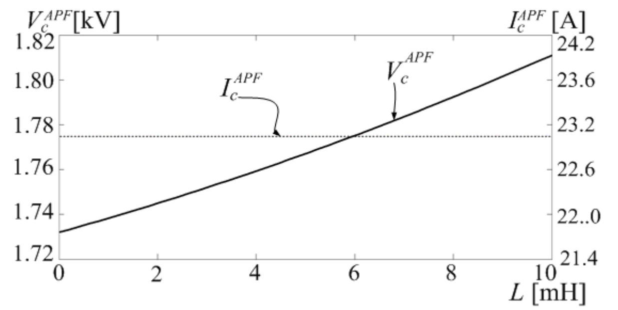

Fig. 3. Rms voltage and rms current of APF inverter versus L (V_{LL} = 3000 V, P_{out} = 300 kW, L_{ac} = 10 mH, and n = 16).

$$V_c^{APF} = \sqrt{\frac{V_{LL}^2}{3} + \frac{2P_{out}X_{L1}\tan(\varphi)}{3} + \left(\frac{P_{out}X_{L1}}{\sqrt{3}V_{LL}\cos(\varphi)}\right)^2\left(\sin^2(\varphi) + \frac{K_2}{M_L^2}\right)}. \tag{10}$$

where:

$$K_2 = \sum_{m=1}^{n/2}k^2(a_k^2 + b_k^2)\;,\; k = 6m \mp 1.$$

where X_{L1} is the reactance of the filter inductor ($X_{L1} = \omega L$). The APF rating S_{APF}, obtained from (8), (9), and (10), depends on the source voltage V_{LL}, the output power P_{out}, the filtering inductance L, the load input inductance L_{ac}, and the number of harmonics n in the distorted load current to be compensated by the APF.

Fig. 3 plots the rms current through the APF inverter (I_c^{APF}) and the rms voltage its ac-side (V_c^{APF}) versus L. It is observed that I_c^{APF} is kept constant since this current contains the compensating reactive and harmonic currents present in the nonlinear load, which remains constant regardless of the value of L. Nevertheless, V_c^{APF} increments with an increasing L due to the rise of the reactance X_L. This results in a higher ac-side voltage of the APF inverter in order to keep constant the compensating reactive and harmonic currents flowing through L. Consequently, the APF inverter rating S_{APF} is directly proportional to the value of V_c^{APF}.

B. kVA Rating Analysis of HPF Inverters

A HPF system in practical cases operates its inverter as a harmonic compensator. However, an approach to provide reactive power compensation by the HPF inverter has been presented in a recent study [13]. The ac-side voltage of the HPF inverter (v_c^{HPF}) operating only as the harmonic compensator, contains no fundamental component, resulting in a lower ac-side voltage and accordingly in a lower dc-link voltage than the APF inverter. However, unlike APF systems, because the phase angle between the source voltage and the source current is determined by the reactive compensation of the tuned PPF, unity power factor operation at the grid is not guaranteed. The sinusoidal source current in Fig. 2 (c) with the power factor angle θ is given by:

$$i_s^{HPF}(\omega t) = \sqrt{\frac{2}{3}}\frac{P_{out}}{V_{LL}\cos(\theta)}\cos(\omega t - \theta)\;. \tag{11}$$

The compensating current in the HPF system (i_c^{HPF}) in Fig. 1 (b) can be obtained with (4) and (11). The rms values of the HPF inverter current and the ac-side voltage of the HPF inverter are derived as (12) and (13), respectively. Where X_{C1} is the reactance of the PPF capacitor (X_{C1}=1/(ωC)) and:

$$K_3 = \sum_{m=1}^{n/2} \frac{1}{k^2}\left(a_k^2 + b_k^2\right),\ k = 6m \mp 1 .$$

Note that in the case with a unity power factor at the grid (θ =0) and no PPF capacitance (X_{C1} = 0), the rms values of the HPF inverter, (12) and (13), are equal to those of the APF inverter, (9) and (10), respectively. From (12) and (13), the rating of the inverter of the HPF (S_{HPF}) is given by:

$$S_{HPF} = 3V_c^{HPF} I_c^{HPF} . \tag{14}$$

Because the rms values of (12) and (13) are derived without the constraint of the HPF inverter serving as only a harmonic compensator, the rating of the HPF inverter given by (14) with (12) and (13) is valid for the case where both the HPF inverter and the PPF provide arbitrary reactive power compensation. However, in practice, the HPF inverter only compensates for the harmonic currents. Therefore, the kVA rating of the HPF inverter serving as the harmonic compensator should be derived.

Fig. 4 shows equivalent single-phase circuit of the HPF system at both the harmonic and the fundamental frequencies when the inverter operates as a harmonic compensator. In the equivalent circuit at the harmonic frequencies, as shown in Fig. 4(a), the harmonic currents generated by the HPF inverter (i_{ch}^{HPF}) have to track the same harmonic currents in the load (i_{Lh}) with opposite direction of flow. Because i_{ch}^{HPF} is constant and the load condition is fixed, varying the values of the PPF components results in changes in v_c^{HPF}. From the equivalent circuit at the fundamental frequency in Fig. 4(b), the fundamental current through the HPF system (i_{cf}^{HPF}) changes if the PPF values vary. v_s drops completely across the PPF, and the current through the PPF is:

$$i_{cf}^{HPF}(\omega t) = \sqrt{\frac{2}{3}}\frac{V_{LL}}{(X_{L1} - X_{C1})}\sin(\omega t) . \tag{15}$$

where X_{L1} - X_{C1} is the PPF reactance at the fundamental frequency. The magnitude of i_{cf}^{HPF} in (15) is inversely proportional to the magnitude of the PPF reactance, $|X_{L1} - X_{C1}|$. On the other hand, the reactive component of i_{Lf}, which is quantified by the load DPF angle φ from (4), is given by:

$$i_{Lfq}(\omega t) = \sqrt{\frac{2}{3}}\frac{P_{out}}{V_{LL}}\tan(\varphi)\sin(\omega t) . \tag{16}$$

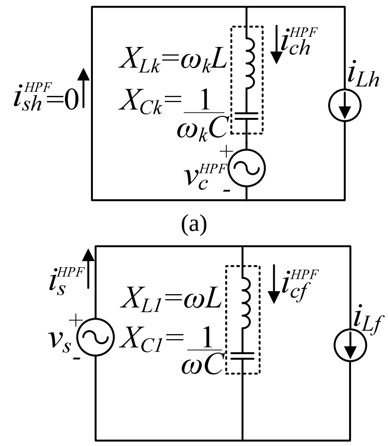

Fig. 4. Equivalent single-phase circuit of HPF system (a) at the harmonic frequencies and (b) at the fundamental frequency.

Vector diagrams of the HPF system working at the fundamental frequency in different operating regions are shown in Fig. 5, where $\boldsymbol{I}_{Lfp}$ and $\boldsymbol{I}_{Lfq}$ denote the active and reactive load current components of an inductive nonlinear load, respectively. These vector diagrams intend to show the reactive compensation at the fundamental frequency caused by the PPF components. As shown in Figs. 5(a)-(c), the compensating current $\boldsymbol{I}_{cf}^{HPF}$ should be in the opposite direction to the load reactive current component $\boldsymbol{I}_{Lfq}$, which requires X_{C1} to be higher than X_{L1} in (15). Otherwise, the PPF is unable to compensate for the load reactive power, as shown in Fig. 5(d). Fig. 5(a) represents the condition of undercompensation (UC), where $\boldsymbol{I}_{cf}^{HPF}$ is smaller than $\boldsymbol{I}_{Lfq}$, resulting in a lagging θ at the grid terminals. Fig.5 (b) shows a HPF system operating at full compensation (FC), leading to unity power factor at the grid terminals. The vector diagram in Fig. 5(c) illustrates overcompensation (OC) by the PPF, where $\boldsymbol{I}_{cf}^{HPF}$ is higher than $\boldsymbol{I}_{Lfq}$ in magnitude, resulting in a leading θ at the grid terminals. However, if X_{C1} is smaller than X_{L1}, in theory the PPF generates a lagging reactive power as seen in Fig. 5(d), which is undesirable.

The fundamental component of the compensating current i_{cf}^{HPF} when the HPF system can compensate both the harmonic and reactive power can be obtained from (4) and (11) as follows:

$$i_{cf}^{HPF}(\omega t) = \sqrt{\frac{2}{3}}\frac{P_{out}}{V_{LL}}\left(\tan(\theta) - \tan(\varphi)\right)\sin(\omega t) . \tag{17}$$

Then by equating (15) and (17), the power factor angle θ

$$I_c^{HPF} = \frac{P_{out}}{\sqrt{3}V_{LL}}\sqrt{\frac{1}{\cos^2(\varphi)} + \frac{1}{\cos^2(\theta)} - 2\left(1 + \tan(\varphi)\tan(\theta)\right) + \frac{K_1}{\left(M_L\cos(\varphi)\right)^2}} . \tag{12}$$

$$V_c^{HPF} = \sqrt{\frac{V_{LL}^2}{3} + \frac{2P_{out}\left(X_{C1} - X_{L1}\right)}{3}\left(\tan(\theta) - \tan(\varphi)\right) + \left(\frac{P_{out}\left(X_{L1} - X_{C1}\right)}{\sqrt{3}V_{LL}}\right)^2\left[\frac{1}{\cos^2(\varphi)} + \frac{1}{\cos^2(\theta)} - 2\left(1 + \tan(\varphi)\tan(\theta)\right) + \frac{K_2X_{L1}^2 - 2K_1X_{L1}X_{C1} + K_3X_{C1}^2}{\left(M_L(X_{L1} - X_{C1})\cos(\varphi)\right)^2}\right]} \tag{13}$$

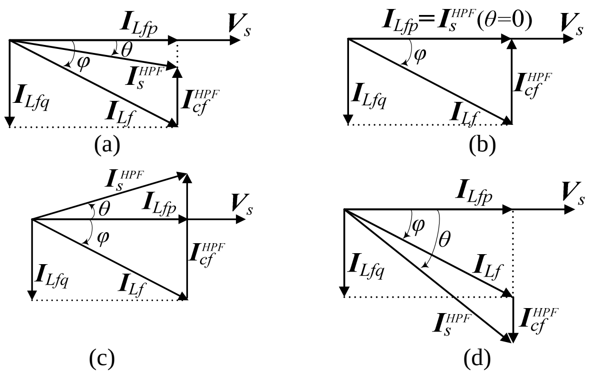

Fig. 5. Vector diagrams of HPF system at the fundamental frequency for inductive nonlinear loads: (a) undercompensation, (b) full-compensation, (c) overcompensation, and (d) undesired operation ($X_{C1} < X_{L1}$).

generated only by means of the PPF components is calculated as:

$$\theta = \tan^{-1}\left(\tan(\varphi) + \frac{V_{LL}^2}{P_{out}(X_{L1} - X_{C1})}\right). \tag{18}$$

The PPF capacitance capable of producing the FC operation is obtained, with $\theta = 0$ in (18), as:

$$C_{FC} = \frac{P_{out}\tan(\varphi)}{\omega V_{LL}^2 + \omega^2 L P_{out}\tan(\varphi)}. \tag{19}$$

The expression for the PPF capacitance for the FC in (19) can be also achieved by equating (15) and (16). After deriving the expressions related to the reactive compensation of the PPF components, it is possible to derive the rms current and voltage of the HPF inverter operating as a harmonic compensator by replacing θ derived in (18) into the more general equations (12) and (13). As a result, it is possible to obtain:

$$I_c^{HPF} = \frac{P_{out}}{\sqrt{3}V_{LL}}\sqrt{\left(\frac{V_{LL}^2}{P_{out}(X_{C1} - X_{L1})}\right)^2 + \frac{K_1}{\cos^2(\varphi)}}. \tag{20}$$

$$V_c^{HPF} = \frac{P_{out}}{\sqrt{3}V_{LL}\cos(\varphi)}\sqrt{K_2 X_{L1}^2 - 2K_1 X_{L1} X_{C1} + K_3 X_{C1}^2}. \tag{21}$$

With (20) and (21), the rating of the HPF inverter that compensates the harmonic currents is given with (14). This new rating is a function of the source voltage V_{LL}, the output power P_{out}, the PPF inductance L, the PPF capacitance C, the input load inductance L_{ac}, and the number of harmonics to be compensated n.

Fig. 6 (a) plots the rms current through the HPF inverter (I_c^{HPF}) and the rms voltage at its ac-side (V_c^{HPF}) versus C. It is seen that I_c^{HPF} rises with the increase of C because the magnitude of the PPF reactance at the fundamental frequency, as shown in (15) decreases, leading to a higher fundamental reactive current flowing through the inverter. On the other hand, since the ac-side voltage of the HPF inverter only generates harmonic voltages, V_c^{HPF} depends on the changes in the PPF reactance at the harmonic frequencies ($|X_{Lk}$ - $X_{Ck}|$)

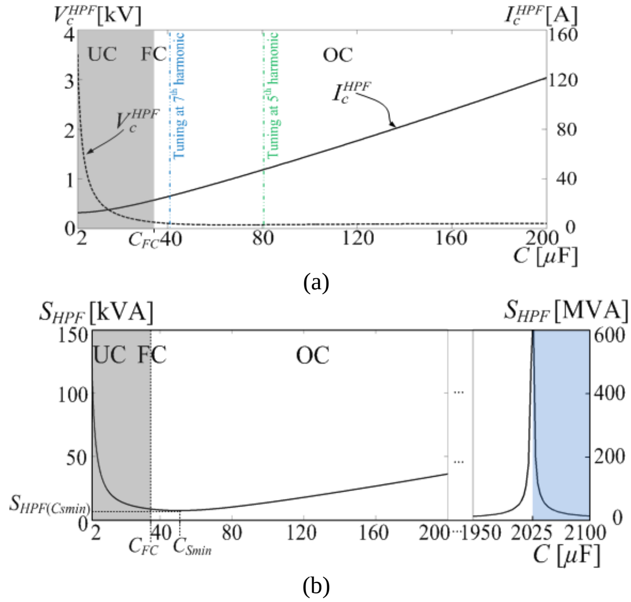

Fig. 6. (a) Rms voltage and rms current and (b) rating of HPF inverter versus C (V_{LL} = 3000 V, P_{out} = 300 kW, L = 5 mH, L_{ac} = 10 mH, and n = 16).

shown in Fig. 4(a). At low values of C, X_{Ck} is very high. This leads to a very high PPF reactance at the harmonic frequencies. Therefore, V_c^{HPF} is quite high, as shown in Fig. 6 (a). This allows the compensating current to flow through the PPF reactance at harmonic frequencies. Increasing C reduces V_c^{HPF}, because a lower voltage at the ac-side of the inverter is sufficient to generate the required compensating current. Based on I_c^{HPF} and V_c^{HPF}, the HPF inverter rating S_{HPF} obtained by (14), (20), and (21) is plotted in Fig. 6(b) as a function of C. It should be noted that the HPF system changes its operating conditions from the UC though the FC to the OC region, with the rise of C. From Fig. 6(b), S_{HPF} with a very small C is unacceptably high owing to its considerably high V_c^{HPF}, as shown in Fig. 6(a). The increasing C, in the low range of the UC region, rapidly decreases S_{HPF} due to the rapid reduction of V_c^{HPF}. S_{HPF} continuously decreases with an increasing C until it reaches the minimum inverter rating $S_{HPF(Csmin)}$ at the capacitance C_{Smin}. When C increases beyond C_{Smin}, S_{HPF} gradually increases owing to the increase of I_c^{HPF}, as shown in Fig. 6(a). At C=2025 μF, the PPF reactance at the fundamental frequency becomes zero, which leads to resonance causing the highest S_{HPF}. At the resonance and its vicinity, shown in the right side of Fig. 6(b), I_c^{HPF} — and accordingly, S_{HPF} —is unacceptably high. Beyond the resonance, in the region represented by the shaded area in the right side of Fig. 6(b), the HPF system goes into the undesirable region shown in Fig. 5(d). This result suggests that the PPF capacitance selected must be as small as possible to reduce the current rating. However, it should be large enough to reduce the voltage rating of the HPF inverter. Consequently, a very large C is not used in practice, yet the

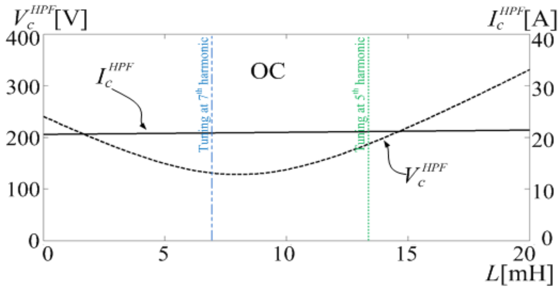

Fig. 7. Rms voltage and rms current of HPF inverter versus L (V_{LL} = 3000 V, P_{out} = 300 kW, C = 30 μF, L_{ac} = 10 mH, and n = 16).

analysis of this case is presented.

Fig. 7 shows I_c^{HPF} and V_c^{HPF} as a function of the PPF inductance L. The system parameters used for Fig. 7 result in the HPF system operating in the OC region, as shown in Fig. 5 (c). The I_c^{HPF} increases very slightly with an increasing L because variations in L have a negligible effect on the decrease of the PPF reactance at the fundamental frequency in comparison to the change in C shown in Fig. 6. On the other hand, a plot of V_c^{HPF} versus L has a parabolic shape because of the changes in the PPF reactance at the harmonic frequencies in Fig. 4(a). At low values of L, X_{Lk} is smaller than X_{Ck}. This yields a negative PPF reactance at harmonic frequencies. When L increases, X_{Lk} increases while X_{Ck} remains constant, which results in lowering the magnitude of the PPF reactance at the harmonic frequencies. Thus, V_c^{HPF} drops owing to the reduction in the PPF magnitude at the harmonic frequencies until it reaches its minimum point. Increasing L beyond this point increases the PPF reactance at the harmonic frequencies. This leads to the need for a higher rms voltage in the ac-side of the HPF inverter. In consequence, the HPF inverter rating S_{HPF} is proportional to V_c^{HPF} with the varying of L.

IV. Comparison of the APF and HPF Inverter Ratings

In the previous section, the analytical derivations of the ratings for APF and HPF systems and the effects of the reactive components L and C on the inverter rantings were analyzed. In this section, APF and HPF inverter rating comparisons are carried out in terms of the harmonics to eliminate n, the load input inductance L_{ac}, the output power P_{out}, and the filtering inductance L. Because a practical HPF system should operate with a fixed PPF capacitance, unity power factor operation cannot be achieved in the whole range of the comparisons. It should be noted, for this comparison, that the APF always operates at unity power factor.

Fig. 8(a) and (b) shows the inverter ratings of the APF and the HPF systems plotted against the number of harmonics to eliminate, n. Accordingly to the number of harmonics eliminated by the filters, the THD in the current at the grid

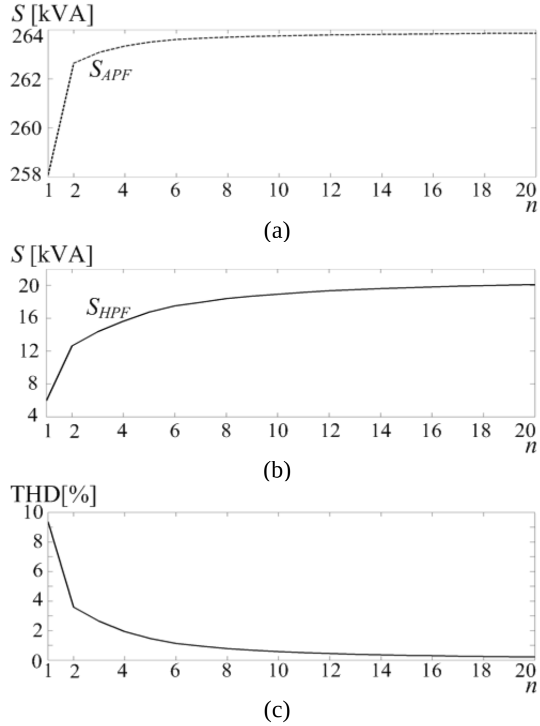

Fig. 8. (a), (b) Inverter ratings and (c) associated THD versus n (V_{LL} = 3000 V, P_{out} = 500 kW, L = 7 mH, C = 76.8 μF, and L_{ac} = 10 mH).

terminals is displayed in Fig. 8(c). It can be seen that improving the current quality at the grid causes both S_{APF} and S_{HPF} to increase with an increasing n since the currents and voltages of the inverters contain harmonic components n. As a result, more harmonic power is provided by the inverters. Nevertheless, S_{APF} has a much larger rating than S_{HPF} due to the continuous reactive compensation that the APF inverter has to provide. For instance, when n=1, S_{APF} is already close to the value of the rating when n=20 because the reactive compensation takes a large part of the power in the APF inverter. The IEEE 519 harmonic current constraints are met up to the 49th harmonic in the source current, which leads to n =16, which is used in the further comparisons.

Fig. 9(a) and (b) shows the inverter ratings and power factors of the APF and the HPF systems plotted against the ac inductance of the diode rectifier L_{ac}. Increasing L_{ac} reduces di_L/dt owing to the load current commutations, which results in smoother harmonic currents that decrease the voltage spikes on the inverter ac-side. Therefore, both the APF and HPF inverter ratings decrease with an increasing L_{ac} in the low-inductance region. However, the load reactive power also increases with an increasing L_{ac} as seen in Fig. 2 (d). Because the APF inverter has to compensate for the load reactive power, S_{APF} first decreases due to a di_L/dt reduction and then increases with a larger L_{ac} due to the increased load reactive power to be compensated. In the meantime, S_{HPF} continues to decrease with an increasing of L_{ac}, owing to the

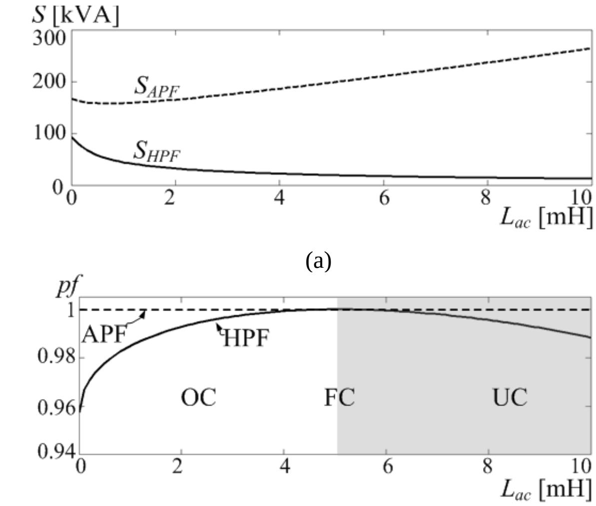

Fig. 9. (a) Inverter ratings and (b) power factor versus L_{ac} (V_{LL} = 3000 V, P_{out} = 500 kW, L = 7 mH, C = 52 μF, and n = 16).

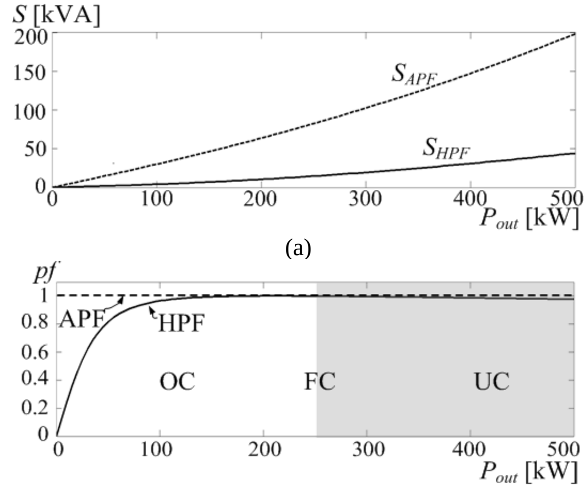

Fig. 10. (a) Inverter ratings and (b) power factor versus P_{out} (V_{LL} = 3000 V, L_{ac}= 5 mH, L = 7 mH, C = 15 μF, and n = 16).

absence of reactive power compensation by the inverter. The HPF system works in the OC region with L_{ac} = 0, as shown in Fig. 9 (b). This is because the reactive component of the load current $\boldsymbol{I}_{Lfq}$ is zero with L_{ac} = 0 and the fundamental current $\boldsymbol{I}_{cf}^{HPF}$ generated by the PPF drives the HPF system into the OC region, as shown in Fig. 5(c). When L_{ac} is increased, the reactive power in the load increases. Thus, the HPF goes through the FC to the UC region.

Fig. 10 depicts the inverter ratings and power factor of the APF and the HPF systems as a function of P_{out}. Both of the inverter ratings increase with an increasing P_{out} due to an increase of the harmonic power to compensate. However, the APF inverter has to compensate for the reactive power as well, which results in larger increments of S_{APF} compared to the increment of S_{HPF}. The increasing P_{out} moves the operating region of the HPF system from the OC region to the UC region, as shown in Fig. 10(b). It is shown that the power factor of the grid terminals with the HPF system is significantly affected by changes in P_{out}.

This is due to the fact that the increase of P_{out} in Fig. 2(d) results in a higher load reactive power while the PPF reactive compensation remains constant resulting in a wide variation of the power factor at the grid.

Fig. 11 illustrates the inverter ratings and the power factor of the APF and HPF systems as a function of L. Note that S_{APF} increases with an increasing L due to the increase of the voltage rating $\boldsymbol{V}_c^{APF}$ as shown in Fig. 3. On the other hand, S_{HPF} first decreases and then increases with an increasing L owing to the reactance change of the PPF at the harmonic frequencies shown in Fig. 7. An increasing L moves the operating condition of the HPF system from the UC region to the OC region, as shown in Fig. 11(b). Notice that the power factor of the grid terminals with the HPF system is insignificantly affected by L. However, L should not be very large in practice to allow the controller of the system to work

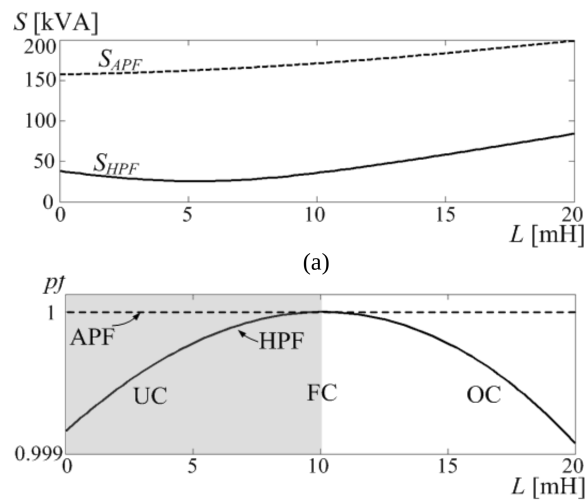

Fig. 11. (a) Inverter ratings and (b) power factor versus L (V_{LL} = 3000 V, P_{out}= 500 kW, L_{ac}= 2 mH, C = 32 μF, and n = 16).

properly. A large L may cause a reduction of the switching frequency and the requirement of an increased dc-link voltage as well as THD deterioration.

V. Analysis and Comparison of the DC-Link Voltage Levels

In this section, the requirements for the dc-link voltage of the APF and HPF inverters are presented and discussed. The required inverter dc-link voltage is typically set to a value that is 5 % higher than its peak line-to-line ac-side voltage. Thus, the peak values of the ac-side voltages can be used to select an appropriate dc-link voltage level. With v_s and the voltage drop across the PPF, the ac-side voltages of both the inverters, v_c^{APF} and v_c^{HPF}, are derived as (22) and (23), respectively.

Fig. 12 shows the ac-side voltage waveforms of v_c^{APF} and v_c^{HPF} for a unity power factor under two different values of L_{ac} for the sake of observing the effect of a variation of C on the ac side voltage of the inverters. This is done because different PPF capacitances are used in Figs. 12(a) and (b) in order to make the HPF system operate at unity power factor. From Fig. 12, it is clear that v_c^{HPF} does not contain a fundamental component, while v_c^{APF} has both fundamental and harmonic components. It can be seen that the voltage spikes in v_c^{APF} with a large L_{ac}, shown in Fig. 12(b), are lower than those in v_c^{APF} with a small L_{ac}, shown in Fig, 12 (a), due to the reduction of di_L/dt during the commutation times of the diode rectifier as can be seen in Fig. 2(a). This results in smoother compensating currents and, as a result, a smoother waveform of the ac side voltage of the APF inverter. The voltage v_c^{HPF} with a large L_{ac} and a large C in Fig. 12(b) is almost 10 times lower than that of Fig. 12(a) with a small L_{ac} and a small C because of the reduction of the PPF impedance due to the increased value of C. This is consistent with Fig. 6 (a) where the rms voltage value of the HPF inverter decreases with an increasing C.

Additionally, the voltage spikes in v_c^{APF} and v_c^{HPF} move towards the right side with a larger L_{ac} as observed in Fig. 10. This is due to the fact that the current commutation interval Δ increases with L_{ac} and shifts the spikes to the right by the time of Δ. It should be noted that the peak value v_c^{HPF} is generally lower than that of v_c^{APF} resulting in a low dc-link voltage of the HPF inverter when compared to the dc-link voltage of the APF inverter. However, with the very small C used in the HPF system, the peak value of the HPF ac-side voltage can be higher than that of the APF ac-side voltage, as shown in Fig. 10 (a). This tells us that it is not desirable to employ a very small C in the design of HPF systems. In fact, in practice, implementing such a small C will equate or overpass the cost of implementation of the HPF to the APF system without a controllable reactive power, which is undesirable. In order to verify the derived equations, (22) and (23), simulations were carried in the PSIM platform. The controllers used for the simulations are found in [17]. The simulation of the ac voltages of the APF and HPF is displayed in Fig. 13, by means of a low pass filter that filters out the switching frequency components. It can be seen that Fig. 13 shows a good relation with Fig 12(b). Since the simulations are operated with controllers that, in practice, cannot suppress entirely the harmonics due to controller’s performance, efficiency, and other factors related to the low pass filter used, the simulated waveforms are not totally similar to the calculated waveforms from Fig. 12. However, the waveform pattern is in concordance between these figures.

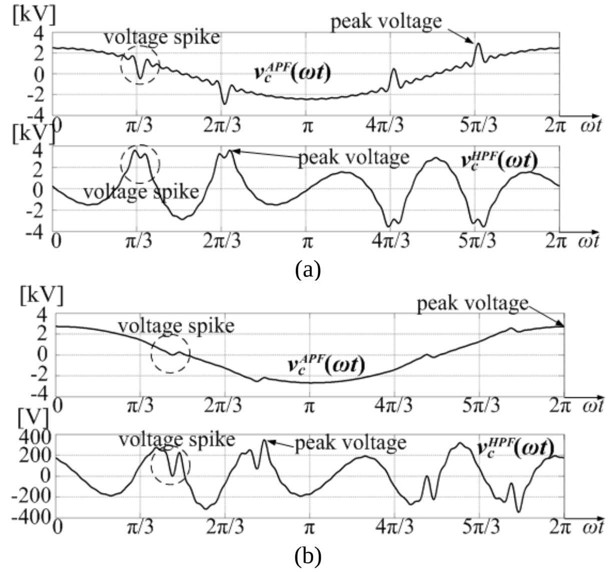

Fig. 12. Ac-side voltages of the APF and the HPF inverters at unity power factor operation (V_{LL} = 3000 V, P_{out} = 300 kW, L = 5 mH, and n=16,) with (a) L_{ac} = 0.2 mH (C_{FC} = 4.5 μF) and (b) L_{ac} = 10 mH (C_{FC} = 35 μF).

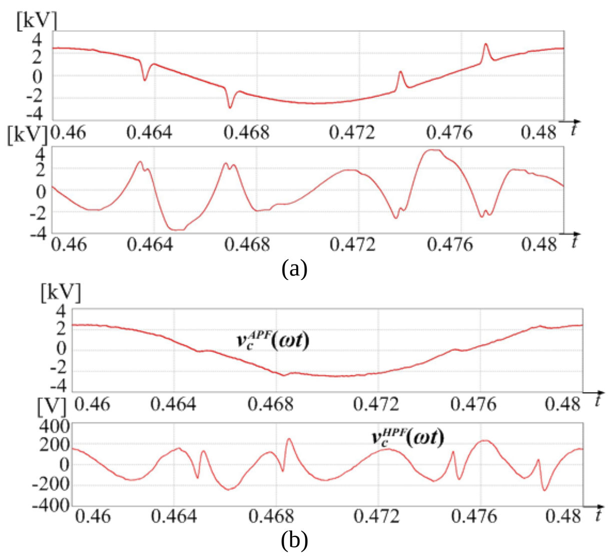

Fig. 13. Circuit simulation of ac-side voltages of the APF and the HPF inverters at unity power factor operation (V_{LL} = 3000 V, P_{out} = 300 kW, L = 5 mH, and n=16,) with (a) L_{ac} = 0.2 mH (C_{FC} = 4.5 μF) and (b) L_{ac} = 10 mH (C_{FC} = 35 μF).

Fig. 14(a) shows the dc-link voltage of the APF (v_{dc}^{APF}) and the HPF (v_{dc}^{HPF}) inverters as functions of P_{out} and L_{ac} in

$$v_c^{APF}(\omega t)=\sqrt{\frac{2}{3}}V_{LL}\cos(\omega t)+\sqrt{\frac{2}{3}}\frac{P_{out}X_{L1}\tan(\varphi)}{V_{LL}}\cos(\omega t)+\sqrt{\frac{2}{3}}\frac{P_{out}}{V_{LL}M_L\cos(\varphi)}\sum_{m=1}^{n/2}(-kX_{L1})(a_k\sin(k\omega t)-b_k\cos(k\omega t))\frac{2}{\sqrt{3}}\cos\left(\frac{k\pi}{6}\right)\sin\left(\frac{k\pi}{2}\right),\ k=6m\mp1. \quad (22)$$

$$v_c^{HPF}(\omega t)=\sqrt{\frac{2}{3}}\frac{P_{out}}{V_{LL}M_L\cos(\varphi)}\sum_{m=1}^{n/2}\left(\frac{X_{C1}}{k}-kX_{L1}\right)(a_k\sin(k\omega t)-b_k\cos(k\omega t))\frac{2}{\sqrt{3}}\cos\left(\frac{k\pi}{6}\right)\sin\left(\frac{k\pi}{2}\right),\ k=6m\mp1\ . \quad (23)$$

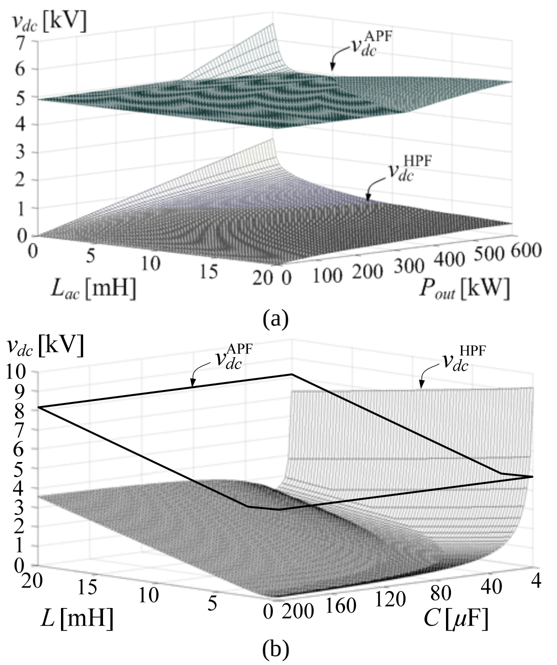

Fig. 14. (a) Dc-link voltages of the APF and HPF inverters versus L_{ac} and P_{out} (V_{LL} = 3300 V, C = 40 μF, L = 3.5 mH, and n = 16). (b) Dc-link voltages of the APF and HPF inverters versus L and C (V_{LL} = 3300 V, P_{out}= 600 kW, L_{ac} = 10 mH, and n = 16).

order to filter up to n=16. The voltages v_{dc}^{APF} and v_{dc}^{HPF} increase with an increasing P_{out}. This is due to the fact that the HPF inverter should generate a higher harmonic voltage with a higher P_{out} and the APF inverter should generate a higher harmonic voltage with a higher voltage for reactive compensation since the reactive power increases with P_{out}. The increase of L_{ac} reduces the voltage spikes in v_c^{HPF}. Thus, the dc-link voltage v_{dc}^{HPF} is lowered. On the other hand, the initial increase of L_{ac} decreases the voltage spikes in v_c^{APF} causing a reduction of v_{dc}^{APF}. However, v_{dc}^{APF} gradually increases with an increasing L_{ac} because, as seen in Fig. 2 (d), the reactive power in the load increases. Thus, the fundamental component of v_c^{APF} needs to be higher to compensate for that reactive power. It is observed that the dc-link voltage v_{dc}^{HPF} is considerably lower than v_{dc}^{APF} in all of the areas of Fig. 14 (a). Fig. 14 (b) shows the dc-link voltages as a function of L and C. The voltage v_{dc}^{APF} rises with an increasing of L as seen in Fig. 3, where the ac side rms current increases with L. The voltage v_{dc}^{HPF} also increases with L when C is large enough. This relates to the right side of V_c^{HPF} in Fig.7. Nevertheless, an increasing L reduces the required v_{dc}^{HPF} when C is very small, which relates to the left side of Fig.7. However, as previously mentioned a very small C is impractical for implementation. In terms of C, as previously analyzed in Fig. 6, the required v_{dc}^{HPF} is reduced with an increase of C. Yet, when L is very large, an increasing C causes a notorious increase in v_{dc}^{HPF} due to an increase of the PPF reactance at the harmonic frequency, which increases the ac side voltage of the inverter. However, again, very large values of L are impractical.

VI. CONCLUSIONS

This paper has presented a theoretical analysis and comparisons of APF and the HPF systems in terms of the inverter ratings and design features. The ratings of the HPF inverter and the power factor at the grid the terminals in HPF systems are analyzed in detail in terms of the circuit parameters such as the source voltage, output power, and reactive components. The rating of the HPF inverter is sensitive to a variation in the PPF capacitance, whereas the PPF inductance has a reduced effect on it. In addition, the operating regions related to the power factor at the grid terminals of HPF systems move from the UC region through the FC to the OC region, with an increasing PPF capacitance, increasing PPF inductance, decreasing input load inductance, and decreasing load output power. Due to the fixed reactive power compensation by the PPF in HPF systems, the power factor at the grid terminals of the HPF varies considerably when the load output power changes. Thus, in order to maintain power factors close to unity, HPF systems might not be appropriate in areas with a wide variation of the load output power. However, the HPF inverter shows, in general, lower kVA ratings than the APF inverters at the outlined range values of the PPF components. Thus, the HPF inverter, with an appropriate selection of reactive components for reactive power compensation, gives performance that is similar to that of the APF inverter but with a less costly topology. The dc-link voltage requirement is shown to be much lower in the HPF inverter when the capacitance in the PPF is large enough to reduce the reactance of the PPF. This results in savings due to the reduced semiconductor ratings in the HPF inverter and the dc-link capacitor rating.

ACKNOWLEDGMENT

This research was supported by the National Research Foundation of Korea (NRF) grant funded by the Korea government (MSIP) (2014R1A2A2A01006684) and the Human Resources Development (No.20154030200860) of the Korea Institute of Energy Technology Evaluation and Planning (KETEP) grant funded by the Korea government Ministry of Trade, Industry and Energy.

REFERENCES

[1] F. Z. Peng, H. Akagi, and A. Nabae, “A new approach to harmonic compensation in power systems- a combined system of shunt passive and series active filters,” *IEEE Trans. Ind. Appl.*, Vol. 26, No. 6, pp. 983-990, Nov./Dec. 1990.

[2] H. J. Azevedo, J. M. Ferreira, A. P. Martins, and A. S. Carvallo, “An active power filter with direct current control for power quality conditioning,” *Electric Power*

Components and Systems, Vol. 36, No. 6, pp. 587-601, May 2008.

[3] Y. Wang and Y. X. Xie, "Adaptive DC-link voltage control for shunt active power filter," *Journal of Power Electronics*, Vol. 14, No. 4, pp. 764-777, Jul. 2014.

[4] M. Rukonuzzman and M. Nakaoka, "An advanced three-phase active filter with adaptive neural network based harmonic detection scheme," *Journal of Power Electronics*, Vol. 2, No. 1, pp. 1-10, Jan. 2002.

[5] P. Acuna, L. Moran, M. Rivera, J. Dixon, and J. Rodriguez, "Improved active power filter performance for renewable power generation systems," *IEEE Trans. Power Electron.*, Vol. 29, No. 2, pp. 687-694, Feb. 2014.

[6] S. Bhattacharya, T. M. Frank, D. M. Divan, and B. Banerjee, "Active filter system implementation," *IEEE Ind. Appl. Mag*., Vol. 4, No. 5, pp. 47-63, Sep./Oct. 1998.

[7] S. Kim and P. N. Enjeti, "A new hybrid active power filter (APF) topology," *IEEE Trans. Power Electron*., Vol. 17, No. 1, pp. 48-54, Jan. 2002.

[8] Y. Wang, Y. X. Xie, and X. Liu, "Analysis and design of DC-link voltage controller in shunt active power filter," J*ournal of Power Electronics*, Vol. 15, No. 3, pp. 763-774, May 2015.

[9] T. C. Green and J. H. Marks, "Ratings of active power filters," *IEE Proceedings - Electric Power Applications*, Vol. 150, No. 5, pp. 607-614, Sep. 2003.

[10] S. Kwak and H. A. Toliyat, "Design and rating comparisons of PWM voltage source rectifiers and active power filters for AC drives with unity power factor," *IEEE Trans. Power Electron.*, Vol. 20, No. 5, pp. 1133-1142, Sep. 2005.

[11] C. S. Lam, X. X Cui, W. H. Choi, M. C. Wong, and Y. D. Han, "Minimum inverter capacity design for LC-hybrid active power filters in thre-phase four-wire distribution systems," *IET Power Electronics*, Vol. 5, No. 7. pp. 956-968, Aug. 2012.

[12] B. Gutierrez and S. Kwak, "Comparative analysis of APF and HPF for utility harmonic compensation", in 9th International Conference on Power Electronics and ECCE Asia (ICPE-ECCE Asia), 2015.

[13] S. Rahmani, A. Hamadi, and K. Al-Haddad, "A lyapunov-function-based control for three-phase shunt hybrid active filter," *IEEE Trans. Ind. Electron.*, Vol. 59, No. 3, pp. 1418-1429, Mar. 2012.

[14] G. Bhuvaneswari and M. G. Nair, "Three-phase hybrid shunt filters for power quality improvement," *Journal of Power Electronics*, Vol. 7, No. 3, pp.257-264, 2007.

[15] L. Jianben, C. Qiaofu, and T. Jun, "A novel DC voltage control strategy of series hybrid active power filter," *International Journal of Electronics*, Vol. 100, No. 10, pp. 1414-1428, Dec. 2012.

[16] H. Akagi, S. Srianthumrong, and Y. Tamai, "Comparisons in circuit configuration and filtering performance between hybrid and pure shunt active filters," in *38th Industry Applications Conference (IAS) Annual Meeting*, Vol. 2, pp. 1195-1202, Oct. 2003.

[17] S. Srianthumrong and H. Akagi, "A medium-voltage transformerless AC/DC power conversion system consisting of a diode rectifier and a shunt hybrid filter," *IEEE Trans. Ind. Appl*., Vol. 39, No. 3, pp. 874-882, May/Jun. 2003.

[18] Y. Li and G. Li, "A novel hybrid active power filter with a high-voltage rank," *Journal of Power Electronics*, Vol. 13, No. 4, pp. 719-728 , Jul. 2013.

[19] C. S. Lam, W. H. Choi, M. C. Wong, and Y. D. Han, "Adaptive dc-link voltage controlled hybrid active power filters for reactive power compensation," *IEEE Trans. Power Electron.*, Vol. 27, No. 4, pp. 1758-1772, Apr. 2012.

[20] N. Mohan, T. M. Undeland, and W. P. Robbins, *Power electronics, converters applications and design*, John Wiley & Sons, Third ed., New York, 2003.

Bryan Gutierrez was born in Lima, Peru, in 1988. He received his B.S. degree in Electronics Engineering from Pontificia Universidad Catolica del Peru, Lima, Peru, in 2012. He is working presently working towards his M.S. degree in Electrical and Electronics Engineering at Chung-Ang University, Seoul, Korea. His current research interests include the analysis and control of hybrid active power filters, and multilevel converters.

Sang-Shin Kwak received his Ph.D. degree in Electrical Engineering from Texas A&M University, College Station, TX, USA, in 2005. He worked as a Research Engineer at LG Electronics, Changwon, Korea, from 1999 to 2000. He was also with the Whirlpool R&D Center, Benton Harbor, MI, USA, in 2004. He worked as a Senior Engineer in the Samsung SDI R&D Center, Yongin, Korea, from 2005 to 2007. He worked as an assistant professor at Daegu University, Gyeongsan, Korea, from 2007 to 2010. He has been with Chung-Ang University, Seoul, Korea since 2010, where he is presently working as an Associate Professor. His current research interests include the topology design, modeling, control, and analysis of AC/DC, DC/AC, and AC/AC power converters, including the resonant converters for adjustable speed drives and digital display drivers, as well as modern control theory applied to DSP-based power electronics.